Wavelength-Dependent Conformational Changes in Collagen after Mid-Infrared Laser Ablation of Cornea

Yaowu Xiao,* Mingsheng Guo,† Peng Zhang,‡ Ganesh Shanmugam,‡ Prasad L. Polavarapu,‡ and M. Shane Hutson*

*Department of Physics and Astronomy and Vanderbilt Institute for Integrative Biosystem Research and Education, Vanderbilt University, Nashville, Tennessee 37235; †Department of Physics, Fisk University, Nashville, Tennessee 37208; and ‡Department of Chemistry, Vanderbilt University, Nashville, Tennessee 37235

ABSTRACT We ablated porcine corneas with a free electron laser tuned to either 2.77 or 6.45 μm, two matched wavelengths that predominantly target water and protein, respectively. The ejected nonvolatile debris and the crater left behind were examined by circular dichroism, Raman spectroscopy, and scanning electron microscopy to characterize the postablation conformation of collagen proteins. We found near-complete unfolding of collagen secondary and tertiary structure at either ablating wavelength. On the other hand, we found excess fibril swelling and evidence for excess *cis*-hydroxyproline in the 6.45-μm debris. These results support the hypothesis that the favorable ablative properties of protein-targeting wavelengths rest on selective heating of tissue proteins.

INTRODUCTION

Soft tissue ablation with mid-infrared (IR) free electron lasers (FEL) displays a strong, and yet odd, wavelength dependence (1). The strongest absorption by soft tissues occurs near 3 μm, but radiation in the 6-μm region is able to cut tissue more efficiently and with remarkably little collateral damage. Based on this, surgeons have successfully used an FEL operating at 6.45 μm in both human ophthalmic surgery and neurosurgery (2–4). Mechanistically, tissue removal with nanosecond- and microsecond-pulsed mid-IR lasers is driven by the explosive vaporization of water (5). Expansion of this vaporized water is constrained, and tissue removal ultimately depends on a structural failure of the protein matrix. Attempts to explain the odd wavelength dependence above have thus invoked a wavelength-dependent loss of protein structural integrity (1,6–8), where targeting protein vibrations in the 6-μm region weakens the tissue matrix, prevents the buildup of a large pressure head, and allows tissue removal to commence at lower energy densities (6). In accord with this hypothesis, we have recently shown that FEL ablation of corneas leads to a wavelength-dependent scission of the dominant matrix protein, fibrillar collagen I (9).

The previous models for FEL ablation further suggested a multistep chain of events that leads to the loss of protein structural integrity (6–8). First, the nanoscale heterogeneity of tissues leads to wavelength-dependent ''hot spots'' in water for wavelengths near 3 μm and in the protein matrix for the 6-μm region. Second, these protein hot spots enable a much faster rate of thermal collagen denaturation. This faster rate leads to a larger accumulation of denatured collagen at the moment explosive vaporization begins. This moment is crucial because, as the vapor expands, the protein matrix is stressed. Collagen denaturation makes the protein matrix brittle, lowers the tissue's ultimate tensile strength (10), and allows vaporization-driven mechanical fragmentation at lower stresses (6). To test these models, we have subjected the debris ejected from corneas during ablation to a careful postablation analysis. Previous postablation analyses of the debris have noted that the particle size (11) and the degree of collagen fragmentation (9) were strongly wavelength dependent, but the evidence for collagen conformational changes was inconsistent. High amide I frequencies in FTIR spectra suggested a native conformation in the debris, but ^{13}C-NMR spectra suggested substantial *trans*-to-*cis* isomerization of proline residues, incompatible with the native triple-helical structure of collagen. In this article, we provide additional analysis of proteins in the ablation debris to resolve these inconsistencies and to delineate the wavelength dependence of collagen conformational changes after mid-IR ablation.

Fibrillar collagens have a highly hierarchical structure. The individual polypeptide chains possess an $(X\text{-}Y\text{-}Gly)_n$ pattern along a ~1000-residue domain, where the X and Y positions are often occupied by proline and hydroxyproline residues. The rigid ring structure of these imino acids favors the dihedral angles of a polyproline-II (PPII) helix provided that all the peptide bonds are in a *trans*-configuration. The PPII structure yields characteristic features in vibrational circular dichroism (VCD) spectra (12); and the *trans*- versus *cis*-configurations are identifiable through solution-state Raman (13) and ^{13}C-NMR spectra (14). At the next structural level, three collagen polypeptide chains associate to form a right-handed triple-helical structure. The presence of this longer-range tertiary structure can be probed by ultraviolet circular dichroism (UVCD) (15). Finally, these triple helices bundle together into a staggered and cross-linked array to

Submitted June 5, 2007, and accepted for publication September 24, 2007.

Address reprint requests to M. Shane Hutson, Vanderbilt University, Station B No. 351807, Nashville, TN 37235. Tel.: 615-343-9980; Fax: 615-343-7263; E-mail: shane.hutson@vanderbilt.edu.

Editor: Brian R. Dyer.

0006-3495/08/02/1359/08 $2.00

doi: 10.1529/biophysj.107.114389

form long collagen fibrils. The fibril morphology can be probed with several techniques, including scanning electron microscopy (SEM). A subset of these techniques has been used previously to investigate collagen conformational changes after diode-laser welding of rat tail tendons (16).

In this study, we ablate porcine corneas with a FEL at two wavelengths for which cornea has the same absorption coefficient, but which predominantly target two different chromophores. At 6.45 μm, the laser energy is absorbed in part by the low-frequency wing of the water-bending mode (centered at 6.1 μm) and in part by the amide II mode of proteins. The energy is not exclusively targeted to protein, but the protein/water absorption ratio is higher here than at any other peak in the mid-IR. At 2.77 μm, the laser energy is largely absorbed by the high-frequency wing of the water OH-stretching mode with a small amount of absorption by protein OH- and NH-stretching modes. Among the limited set of wavelengths that are both accessible to the Vanderbilt FEL and for which cornea has the same absorption coefficient as at 6.45 μm, the smallest protein/water absorption ratio occurs at 2.77 μm. After ablation at either wavelength, the techniques described above (VCD, UVCD, Raman, SEM) were used to probe the conformation of collagen proteins in the ejected debris. We also used Raman spectroscopy to analyze collagen proteins in and around the ablation craters. We find that individual polypeptide chains are unfolded and triple-helix structure is lost after ablation at either wavelength; however, wavelength-dependent differences are observed in the degree of fibril swelling and in the amount of *trans*-to-*cis* proline isomerization.

MATERIALS AND METHODS

Tissue ablation

To collect ablation debris, the central region of an excised strip of cornea was irradiated by an FEL through a CaF_2 window. As described previously (9), this window captured the nonvolatile debris as it was ejected from the tissue surface. All ablations and debris collections were performed in an air atmosphere, and the corneal surface was repeatedly dabbed with saline drops to maintain near native hydration. The gap between the corneal surface and the CaF_2 window was ~0.5 mm, and the FEL spot diameter at the sample surface (measured with a knife edge) was ~100 μm. The Vanderbilt Mark-III FEL has a complex pulse structure (17), and the parameters used for ablation were as follows: 1- to 3-ps-long micropulses at a repetition rate of 2.856 GHz; 3- to 5-μs-long macropulses at a repetition rate of 30 Hz and a macropulse energy of ~20 mJ. The exact energy used was adjusted according to the spot-size measurement to yield a consistent macropulse fluence of 240 J/cm^2. For subsequent VCD and UVCD analysis, the sample and window were moved together to collect 30–40 ablation spots per sample/window pair. Each spot was exposed to 5–10 macropulses and spaced at 1.0-mm intervals. For the micro-Raman and SEM analysis, only one spot was ablated per sample using just a single macropulse.

Circular dichroism

VCD spectra were recorded on a commercial Fourier transform VCD spectrometer (BioTools, Jupiter, FL) with a data collection time of 1 h and spectral resolution of 8 cm^{-1}. The spectrometer was modified to eliminate artifacts (18). These modifications were crucial for successful VCD measurements of the ablation debris in situ on the CaF_2 windows. Control spectra were measured from 5-μm-thick slices of native cornea (obtained by freeze-sectioning at −20°C). All samples for VCD spectroscopy were dried at low vacuum (~10^{-2} torr).

UVCD spectra were recorded on a JASCO 860 spectrometer (JASCO, Easton, MD) equipped with an automated temperature controller. Debris spectra were measured in aqueous solution from pooled samples (obtained by washing the CaF_2 windows with distilled water). Control spectra were measured from an aqueous solution of purified collagen. The concentration of the debris and control collagen was determined by measuring the absorbance at 214 nm (19).

SEM

SEM images were collected on a Hitachi scanning electron microscope (Hitachi High Technologies, Schaumburg, IL). Debris images were in situ on the CaF_2 windows. Control images were from freeze-sectioned slices of cornea. Samples for SEM imaging were fixed in 2% formaldehyde, postfixed in 1% osmium tetroxide, dehydrated, critical-point dried, and sputter-coated with gold.

Raman spectroscopy

Raman spectra were recorded on a Jobin Yvon micro-Raman LabRam system (HORIBA Jobin Yvon, Edison, NJ) as described previously (9). Debris spectra were measured in situ on the CaF_2 windows. Spectra of the ablation crater and surrounding areas were measured after single-pulse ablation. After ablation, the corneas were dried in low vacuum (10^{-2} torr). Raman spectra were measured within 3 days of ablation. Even longer-term storage (1 mo) of dried samples in air yielded no observable spectral changes.

Spectra were also measured for heat-treated slices of cornea (5 μm thick, obtained from freeze-sectioning at −20°C). Slices were transferred onto 10 × 10 × 0.5 mm coverslips, air dried, and placed on a hot metallic plate at a given temperature for 9 min. Raman spectra were then recorded over the next 2 min. After removal from the hot plate, samples were allowed to recover to room temperature either in air or under high vacuum (10^{-6} torr). Additional Raman spectra were then measured once the sample reequilibrated (after 1 h for the sample heated to 60°C but up to 1 wk for 200°C).

Raman spectra were also measured for dried films of purified collagen. Films were prepared by dissolving collagen in distilled water at 1 mg/ml either with or without 0.1 M NaCl. An aliquot (0.1 ml) of each collagen solution was transferred onto a clean CaF_2 window and dried in air for 2 h. To delineate spectral changes in the 900–1000 cm^{-1} range more clearly, all Raman spectra were subjected to a single-point baseline correction at 1020 cm^{-1} and then scaled to give a normalized intensity of 1 for the 920 cm^{-1} band.

^{13}C-NMR spectroscopy

NMR measurements were as described previously (9). Purified collagen samples were dissolved in a mixture of d_6-DMSO and water (70:30 v/v), either with or without 0.3 M NaCl. The DMSO was necessary to increase collagen solubility.

Collagen purification

Collagen preparation and purification followed published procedures (20). After collagen isolation via NaCl precipitation, the salt was removed by extensive dialysis against distilled water. The dialyzed sample was lyophilized and stored at 4°C.

RESULTS

Circular dichroism

A comparison of VCD spectra of the in situ ablation debris and a control corneal slice are shown in Fig. 1. The inset

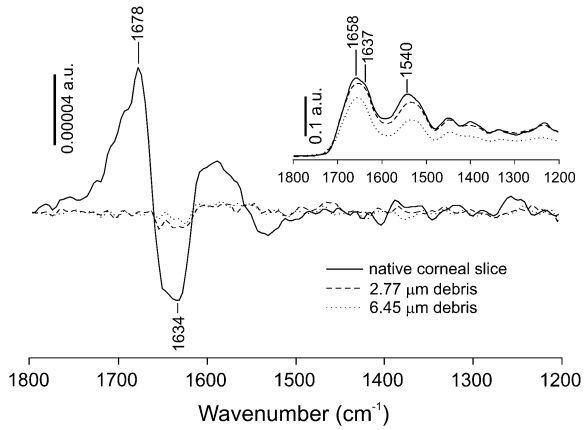

FIGURE 1 VCD spectra of debris collected from ablation of porcine corneas at a wavelength of either 2.77 (*dashed lines*) or 6.45 μm (*dotted lines*). The debris spectra were measured in situ on a CaF_2 window. The VCD spectrum of a dried slice of cornea is shown for comparison (*solid line*). The inset contains the corresponding infrared absorption spectra. Vertical bars mark the scale for each set of spectra in absorbance units.

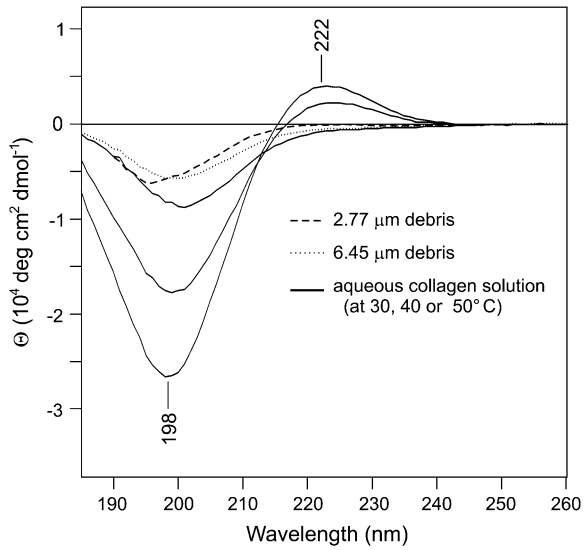

FIGURE 2 UVCD spectra of debris collected from ablation of porcine corneas at a wavelength of either 2.77 (*dashed lines*) or 6.45 μm (*dotted lines*). The debris was resolubilized in distilled water. UVCD spectra of a purified collagen solution at 30°, 40°, and 50°C (*solid lines*) are shown for comparison. The magnitude of the UVCD signals decreases as the collagen triple helices unfold at higher temperatures.

shows the infrared absorption spectra of all three samples and indicates that the path lengths were well matched. The control VCD spectrum, measured for 5-μm-thick slices of native cornea, shows a positive couplet with positive VCD at 1678 cm^{-1} and negative VCD at lower frequency (1634 cm^{-1}). This couplet matches previous VCD spectra of collagen I films (12) and is characteristic of PPII structure. In both debris spectra, the couplet disappears. Thus, laser ablation at either 2.77 or 6.45 μm leads to a complete loss of collagen's native secondary structure.

We further compare the UVCD spectra of purified collagen and resolubilized debris proteins in Fig. 2. The most characteristic UVCD signature for collagen triple helices is a positive band at 222 nm (15). For purified collagen, this positive feature disappears as the collagen solution is heated from 30° to 50°C, indicating the expected thermal denaturation. For the debris proteins, the positive band at 222 nm is absent in both UVCD spectra (collected at 20°C). Thus, laser ablation at either wavelength also leads to an irreversible loss of collagen triple helices. Note that the negative UVCD features in the 200-nm region indicate some residual or reformed structure in the water-soluble debris, structures that are not identical at the two different wavelengths.

SEM

SEM images of the debris fields and a control corneal slice are shown in Fig. 3. Although circular dichroism suggests that the secondary and tertiary structures of fibrillar collagen are lost after ablation, the debris fields still contain higher-order fibril-like structures. These debris-field fibrils do, however, have diameters that are much larger than native collagen fibrils. When data were averaged over 14 distinct fibrils from five different SEM images of corneal slices, the mean native fibril diameter was 42 ± 4 nm. This is just slightly larger than expected (21). Similar averaging from SEM images of the 2.77-μm debris fields yields fibril diameters that are twice as large: 82 ± 11 nm for 17 distinct fibrils from six different images. Fibrils in the 6.45-μm debris fields are even larger: 230 ± 54 nm for 30 distinct fibrils from four different images. Another difference between the native and debris fibrils lies in their spatial distribution. In slices from native corneas and in the 2.77-μm debris, the fibrils are usually found in parallel bundles. This is as expected given the lamellar structure of cornea (21). The isolated fibril in Fig. 3 *b* is an exception that makes the increased diameter of 2.77-μm debris fibrils easier to see. In contrast, isolated fibrils are the rule and not the exception in the 6.45-μm debris.

Raman spectroscopy

Raman spectra of the ablation debris and of the corneal surface in and around the ablation craters are shown in Fig. 4. These spectra were measured after single macropulse ablation at 6.45 or 2.77 μm with a fluence of 240 J/cm^2. The spectral region shown in Fig. 4 is the only one containing significant wavelength-dependent changes. The spectral regions not shown are in good agreement with reference spectra of native corneas (22) and fibrillar collagens (23,24). The dominant features, in particular the amide I (1667 cm^{-1}) and amide III (1243 cm^{-1}) modes, are normally sensitive reporters of protein conformation, but these bands do not appreciably shift between or among any of the debris or crater spectra. As reported previously (9), the 6.45-μm debris

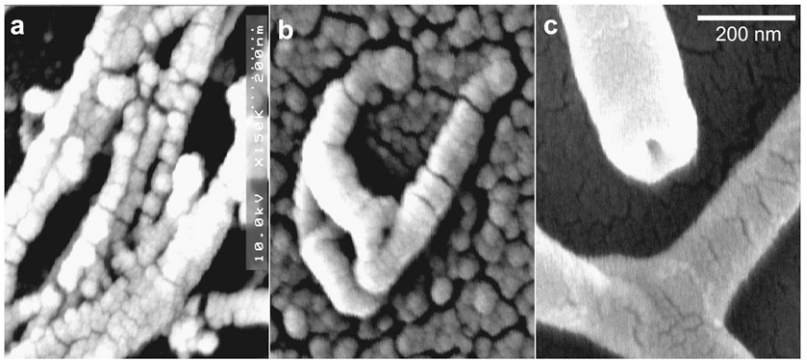

FIGURE 3 Scanning electron micrographs of collagen fibrils in (*a*) slices of unexposed cornea, (*b*) the debris field from 2.77-μm ablation, and (*c*) the debris field from 6.45-μm ablation. The horizontal scale bar is applicable to all three images.

spectrum does contain a Raman band (2249 cm^{-1}) indicative of wavelength-dependent collagen fragmentation. No such Raman band was observed in or around any of the craters.

The Raman spectra do contain subtle differences that depend on the ablating wavelength. In particular, a Raman band at 938 cm^{-1}, the higher-energy and normally higher-intensity component of an overlapping band pair, loses more intensity after ablation at 6.45 μm than at 2.77 μm. We have emphasized this spectral change in Fig. 4 by normalizing the spectra via the lower-energy (920 cm^{-1}) component of the band pair. In spectra from the tissue surface after 2.77-μm ablation, the relative band intensity at 938 cm^{-1} decreases from 1.41 at a location just outside the crater to an average of 1.19 at three locations on the crater rim, side, and bottom. In the corresponding debris spectrum, there is a further decrease to a relative intensity of just 1.03. After 6.45-μm ablation, the relative intensity at 938 cm^{-1} decreases in a similar but stronger fashion. The relative band intensity is already lower just outside the crater (1.31) and decreases further at sites on the crater surface (1.05). In the 6.45-μm debris, the 938 cm^{-1} band disappears almost entirely (relative intensity 0.66). This band has been tentatively assigned to a C-C stretch vibration in either the peptide backbone or the proline ring (23–25), but its relation to protein conformation has not been established.

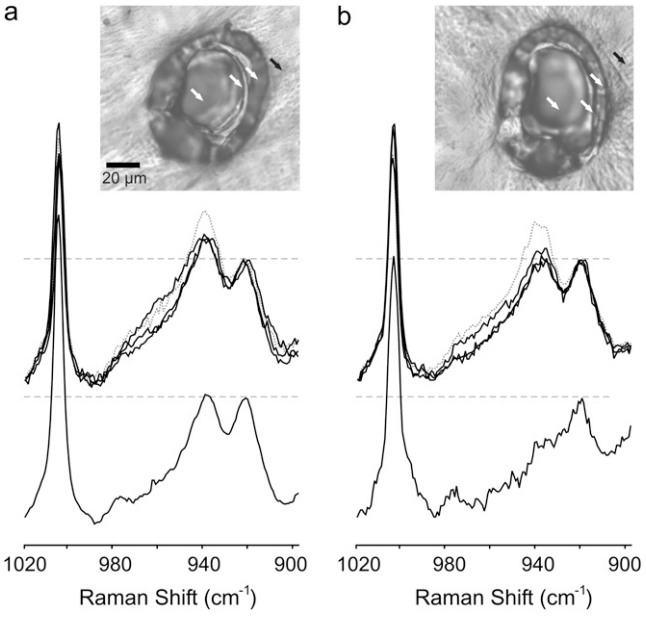

FIGURE 4 Raman spectra of the ablation debris and selected locations in and around the ablation craters. The ablating wavelength was either (*a*) 2.77 μm or (*b*) 6.45 μm. In each panel, the upper spectra are from the locations marked in the inset brightfield images. The dotted shaded curve is from outside the crater (*solid arrow*). The solid curves are from positions on the rim, side, and bottom of the crater (*open arrows*). The lower spectrum in each panel is from the ablation debris. The Raman spectra have all been normalized by the maximum intensity of the 920 cm^{-1} band. The normalized level for each spectrum is marked by a horizontal dashed line. The inset brightfield images are from unstained corneas. The horizontal scale bar (20 μm) is applicable to both images.

To help interpret the Raman spectral differences, we measured additional spectra from heated corneal slices as shown in Fig. 5. The most temperature-sensitive band is the one at 938 cm^{-1}. The relative intensity here decreases as the temperature increases, and by 200°C, this band is no longer even observable. After the samples are returned to room temperature, the relative intensity at 938 cm^{-1} recovers, but incompletely. This intensity loss becomes more irreversible at higher temperatures. Before heating, the relative intensity at 938 cm^{-1} was 1.43. Even after the samples had been allowed to reequilibrate for up to a week, the recovered Raman intensities at 938 cm^{-1} were 1.20, 1.18, 1.10, and 0.86 for heating to 60°, 100°, 150°, and 200°C, respectively. Raman measurements at even higher temperatures were precluded by very high levels of thermally induced fluorescence. All the spectra in Fig. 5 were taken from samples dried in air at room temperature. Interestingly, we observe a further reduction of relative intensity at 938 cm^{-1} if the samples are dried under a vacuum of 10^{-6} torr (not shown). Similar vacuum-drying effects have been reported for collagen and skin (26).

Empirically, the relative Raman intensity at 938 cm^{-1} is indicative of the temperature and hydration history of a sample, but that still tells us little about its relation to collagen structure. Because this band is tentatively assigned to proline vibrations, we also checked whether its intensity is

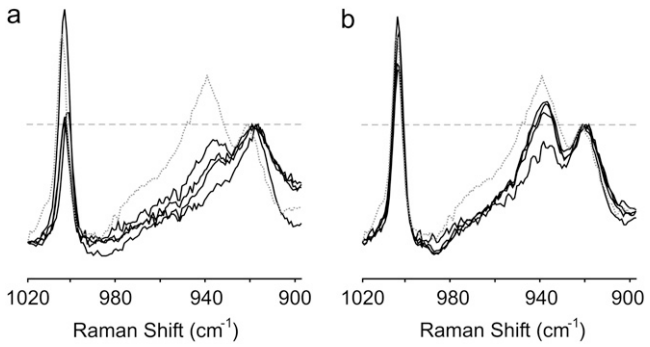

FIGURE 5 Temperature dependence of the 938 cm^{-1} Raman band in dried corneal slices. (*a*) Spectra measured at elevated temperatures of 60°, 100°, 150°, and 200°C; and (*b*) spectra measured after such heating and reequilibration at room temperature. The Raman spectra have all been normalized by the maximum intensity of the 920 cm^{-1} band. This normalized level is marked by the horizontal dashed line. The dotted shaded curve in each panel is from a sample dried at room temperature and never heated. The solid curves are from the heated samples. The intensity at 938 cm^{-1} is largest in the unheated sample and decreases further with each increase in sample temperature.

affected by high salt concentrations known to drive *trans*-to-*cis* proline (and hydroxyproline) isomerization. Raman spectra of collagen films dried from either distilled water or a 0.1 M NaCl solution are shown in Fig. 6, *a* and *b*. The Raman intensity at 938 cm^{-1} (compared with 920 cm^{-1}) is certainly decreased when salt is added. We confirmed that salt addition increased the fraction of *cis*-hydroxyproline via ^{13}C-NMR. As shown in Fig. 6, *c* and *d*, the addition of 0.3 M NaCl increases the intensity of the C_γ resonance of *cis*-hydroxyproline (68 ppm) compared with the *trans* form (70 ppm) (14). Because these Raman and ^{13}C-NMR spectra were measured under different conditions, dried films for Raman

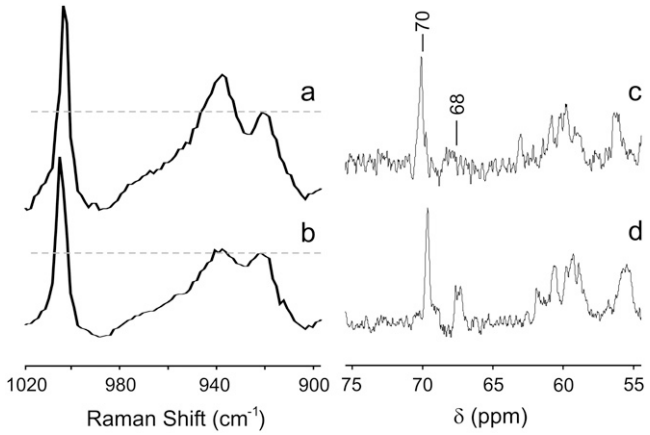

FIGURE 6 Effect of salt concentration on (hydroxy)proline isomerization. (*a* and *b*) Raman spectra are shown for films dried down from a collagen solution in either (*a*) distilled water or (*b*) 0.1 M NaCl. (*c* and *d*) ^{13}C-NMR spectra are shown for collagen solutions in DMSO/water (70:30 v/v) with (*c*) no added salt or (*d*) 0.3 M NaCl. The marked NMR resonances are for *trans*- (70 ppm) and *cis*-hydroxyproline (68 ppm) (14).

and DMSO/water solutions for NMR, one must be careful not to overinterpret the results. Nonetheless, proline and hydroxyproline isomerization is the only protein conformational change we have identified that correlates with the Raman intensity decrease at 938 cm^{-1}.

DISCUSSION

From the above experimental results, we draw two conclusions. First, the collagen proteins in the ablation debris lose nearly all secondary (PPII helix) and tertiary (triple helix) structure regardless of whether the ablation wavelength predominantly targets water (2.77 μm) or protein (6.45 μm) vibrations. This evidence is mainly from the VCD and UVCD spectra. Second, beyond these structural changes, there is evidence that the proteins in the 6.45-μm debris have been subjected to higher temperatures. This evidence is in the form of excess fibril swelling and a reduced Raman intensity at 938 cm^{-1}. The latter may be associated with (hydroxy)-proline *trans*-to-*cis* isomerization.

The evidence for the first conclusion from VCD and UVCD spectra is quite definitive. Note that the debris is dehydrated during the ablation process, and whenever possible, we avoid rehydrating the debris. Doing so could reverse any ablation-induced conformational changes. The VCD measurements were performed on the dried debris in situ on the CaF_2 windows and thus accurately report on the complete lack of secondary structure after ablation. On the other hand, the UVCD measurements required resolubilizing the debris in water and must be more carefully interpreted. The resolubilized debris spectra do have some UVCD features suggesting that some secondary structure has re-formed; however, the signatures of collagen triple helix structure are missing, which suggests that this loss of tertiary structure is irreversible.

The only evidence that seems to be in conflict is our previous set of FTIR debris spectra. These spectra had high amide I frequencies near 1654 cm^{-1} (9), which are not normally associated with unfolded collagen (27). The apparent conflict can be resolved by noting that the association of low amide I frequencies (near 1630 cm^{-1}) with collagen unfolding was made for hydrated samples (27), but our FTIR spectra were measured in situ on the dried debris. The in situ measurement is necessary because rehydrating the debris samples could reverse the secondary structural changes that we are trying to detect. There is little guidance on interpreting amide I frequencies in dried collagenous samples, but our previous measurements on dried corneal slices showed that high amide I frequencies were maintained (9) even when the samples were heated to well above the denaturation temperature of corneal collagen (28). Apparently, the amide I frequency is no longer a reliable reporter of collagen conformation in dried samples. Thus, we discount the FTIR measurements with regard to secondary structure and rely on

the VCD and UVCD spectra to conclude that the collagenous proteins in both sets of ablation debris are unfolded.

The evidence for higher temperatures in the 6.45-μm debris is more indirect. Most importantly, the 6.45-μm debris has a greater loss of Raman intensity at 938 cm^{-1}. Whatever that may imply with regard to structure (see below), the Raman intensity at 938 cm^{-1} decreases as corneal slices are heated. Only part of this decrease is recoverable when the samples return to room temperature, and the amount of recovery decreases as the temperature to which the sample was heated increases. A similar loss of Raman intensity can occur after vacuum drying or at high salt concentrations, but these conditions were well matched in all of the ablation debris samples. Thus, we conclude that proteins in the 6.45-μm debris experienced higher temperatures during the ablation process. We can construct an estimate of the temperatures reached by the debris using the relative intensity at 938 cm^{-1} as a spectral thermometer. If a linear interpolation/extrapolation of the postheating and recovery data from Fig. 5 is used, the 2.77- and 6.45-μm debris spectra are equivalent to heating the samples for 9 min at 170° and 240°C, respectively. Because the debris remains at elevated temperatures for much less than 9 min, this is an underestimate of the maximum temperatures actually reached. The underestimate is likely worse for 6.45 μm, which requires an extrapolation from the current data, because the dependence of recovered intensity at 938 cm^{-1} on temperature becomes steeper as the temperature increases.

In support of the conclusion that the 6.45-μm debris experienced higher temperatures during ablation, the fibrils remaining in the 6.45-μm debris are more isolated and more swollen. Fibrils in the 2.77-μm debris are swollen to approximately twice the native size and are still grouped together in parallel bundles, much as one would expect if the debris consisted of 10- to 100-μm-sized chunks of heat-denatured cornea (11). A similar laser-induced swelling of collagen fibrils has been observed previously (16,29). On the other hand, fibrils in the 6.45-μm debris are not arranged in parallel bundles but are instead isolated and swollen to five times the native size. Although it may seem odd that any fibrils are present after all secondary/tertiary structure has been lost, one must remember that the collagen molecules in a fibril are highly cross-linked. Many of these cross-links are not heat labile and continue to hold the unfolded collagen molecules together, much like a frayed rope. The greater fibril swelling suggests a greater freedom of movement for the unfolded molecules via a greater degree of either cross-link or polypeptide cleavage. This is consistent with our previous results on collagen fragmentation, which is higher in the 6.45-μm debris and which can also be induced to a greater degree by higher temperatures.

The only conformational change we have been able to associate with the Raman intensity loss at 938 cm^{-1} is *trans*-to-*cis* isomerization of (hydroxy)proline. The previously observed fragmentation of collagen does not cause this spectral change. We can reproduce the change under conditions where fragmentation does not occur: temperatures below 200°C, dehydration, and high salt concentration. Each of these conditions may, however, drive (hydroxy)proline isomerization (30,31). In fact, we observe ^{13}C-NMR evidence for an increase of *cis*-hydroxyproline under our high-salt conditions. The most direct way to verify a wavelength-dependent (hydroxy)proline isomerization in the ablation debris would be solid-state ^{13}C-NMR spectroscopy; however, the amount of debris required for such measurements is impractical.

The analysis of the nonvolatile ablation debris presented here has been limited to a single macropulse fluence of 240 J/cm^2. At either 2.77 or 6.45 μm, this fluence is more than 100 times the ablation threshold. Such a high fluence was chosen for three reasons. First, this fluence is in the same range as those used in the original report of high efficiency and low collateral damage for ablation at 6.45 μm (1). Subsequent reports at lower fluence saw a much smaller wavelength dependence in the ablation metrics that largely followed the linear absorption coefficient (11). Second, the photothermal models suggest that any wavelength dependence based on targeting protein versus water would begin to show only for macropulse intensities above 3×10^6 W/cm^2 and would be maximized around 10^9 W/cm^2 (8). The macropulse fluence used here is as high as we can attain on a regular basis and corresponds to macropulse intensities of 5–8 $\times$ 10^7 W/cm^2. Third, our previous analysis found the strongest evidence for wavelength-dependent fragmentation at this same high fluence (9).

Although there are good reasons for choosing a high fluence, this choice does bring several other issues into play, e.g., plasma formation and the continued irradiation of debris proteins in the plume. At a macropulse fluence of 240 J/cm^2, the corresponding peak intensity in the FEL micropulses is between 0.6 and 3×10^{10} W/cm^2. For picosecond pulses, this irradiance is just below the threshold ($>10^{11}$ W/cm^2) for plasma formation in water and soft tissues (32,33). Thermionic plasma formation can occur at lower irradiances, 10^8 to 10^{10} W/cm^2 (5), but the relevant comparison is then to the macropulse irradiance that is also just below threshold. To reduce the chance of plasma formation, we took care to keep the corneal samples fully hydrated. What we could not control were the continued irradiation and dehydration of the debris during the laser pulse. At the very high fluence used here, explosive vaporization is expected to begin just 10–50 ns after the start of a macropulse (6). We do not know if material ejection also begins on the 50-ns time scale, but by the end of a macropulse (at just three times threshold), stroboscopic imaging shows that the plume of water vapor and particulates extend several millimeters from the tissue surface (11). We can be certain that some fraction of the debris is irradiated by part of the macropulse on the way to, and even after contacting, the CaF_2 window; however, we do not know how large a fraction this is. Other stroboscopic imaging studies have shown that material continues to be

ejected from the sample surface well after the end of a macropulse (34). With high fluences and soft tissues, this late recoil-induced material ejection accounts for the overwhelming majority of the mass removed (5).

Comparison to FEL ablation models

Existing models explain the wavelength dependence of soft tissue ablation by a FEL with a multistep process (6–8): the generation of ''hot spots'' by wavelength-dependent selective heating of protein; mechanical weakening of the tissue through a specific thermally activated protein reaction, i.e., collagen denaturation or unfolding; and finally, the explosive vaporization of water and structural failure of the tissue matrix as it attempts to constrain the expanding vapor. Wavelengths that target protein vibrations can have a higher ablation efficiency and lower collateral damage because selectively heating the proteins leads to a weaker tissue matrix at the onset of vaporization.

Our results support a role for the postulated wavelength-dependent selective heating of tissue protein. Specifically, the Raman and SEM results suggest that proteins in the 6.45-μm debris (compared with the 2.77-μm debris) encounter higher temperatures during ablation. Such higher temperatures are also consistent with our previous results on collagen fragmentation in the debris. In each case, we observe that the 6.45-μm debris has an excess accumulation of products from thermally activated protein reactions.

On the other hand, our results cannot confirm the specific involvement of thermally activated collagen denaturation. The models cited above predict the accumulation of collagen denaturation in a wavelength-dependent manner. For wavelengths that target protein vibrations compared with those that target water, the denatured fraction is predicted to be several orders of magnitude higher at the onset of vaporization. Our spectral assessment of collagen denaturation was not made at the moment vaporization began but well after the entire ablation process was complete. At that point, we find complete unfolding of collagen in the debris at both 6.45 and 2.77 μm. This result does not confirm the model predictions, but it may well be a false negative. One would certainly expect collagen denaturation to continue after vaporization. The fact that complete unfolding was seen at both wavelengths means that continued postvaporization unfolding could have erased any earlier evidence of a wavelength dependence. For now, the models' large extrapolations of denaturation kinetics, from milliseconds down to nanoseconds and from 60–100°C to 200–400°C (6), cannot be justified or invalidated. To do so will require time-resolved measurements.

In summary, we have observed three types of structural failures in collagen after mid-IR ablation: 1), the unfolding of local secondary and triple-helix structure; 2), *trans*-to-*cis* (hydroxy)proline isomerization; and 3), the previously observed breakage of the protein backbone at *N*-alkylamide bonds. These structural changes then lead to the swelling of cross-linked collagen fibrils. Interestingly, the wavelength dependence of each reaction follows the height of the relevant energy barriers. The breaking of low-energy hydrogen bonds during unfolding occurs at either wavelength tested; however, the higher activation energy processes of proline isomerization (80–90 kJ/mol (35)) and backbone scission (200–250 kJ/mol (36)) occur preferentially at protein-targeting wavelengths. The results support the hypothesis that selective heating of proteins and the accumulation of thermally activated reaction products occur preferentially at wavelengths in the 6-μm region. The specific role of thermally activated collagen denaturation on nanosecond time scales and its impact on the subsequent ablation dynamics remain to be elucidated.

The authors thank the staff of the W. M. Keck Vanderbilt Free-Electron Laser Center for generously providing beam time and expertise to this project.

This work was supported by grants FA9550-04-1-0045 and FA9620-00-1-0370 from the Department of Defense Medical Free Electron Laser Program; National Science Foundation Human Resources Development grant No. 0420516 (Centers for Research Excellence in Science and Technology); and by the National Science Foundation Center for Biophotonics, managed by University of California, Davis, CA (No. PHY0120999). VCD instrumentation was supported by a grant (to P.L.P.) from the National Science Foundation (CHE0092922).

REFERENCES

1. Edwards, G., R. Logan, M. Copeland, L. Reinisch, J. Davidson, B. Johnson, R. Maciunas, M. Mendenhall, R. Ossoff, J. Tribble, J. Werkhaven, and D. O'Day. 1994. Tissue ablation by a free-electron laser tuned to the amide-II band. *Nature*. 371:416–419.
2. Edwards, G. S., R. H. Austin, F. E. Carroll, M. L. Copeland, M. E. Couprie, W. E. Gabella, R. F. Haglund, B. A. Hooper, M. S. Hutson, E. D. Jansen, K. M. Joos, D. P. Kiehart, I. Lindau, J. Miao, H. S. Pratisto, J. H. Shen, Y. Tokutake, A. F. G. van der Meer, and A. Xie. 2003. Free-electron-laser-based biophysical and biomedical instrumentation. *Rev. Sci. Instrum.* 74:3207–3245.
3. Copeland, M. L., R. J. Maciunas, and G. S. Edwards. 1998. Chapter VII: use of the free-electron laser for metastatic brain tumors. *In* Neurosurgical Topics: Advanced Techniques in Central Nervous System Metastases. R. J. Maciunas, editor. The American Association of Neurological Surgeons, Park Ridge, IL. 113–121.
4. Joos, K. M., J. H. Shen, D. J. Shetlar, and V. A. Casagrande. 2000. Optic nerve sheath fenestration with a novel wavelength produced by the free electron laser (FEL). *Lasers Surg. Med.* 27:191–205.
5. Vogel, A., and V. Venugopalan. 2003. Mechanisms of pulsed laser ablation of biological tissues. *Chem. Rev.* 103:577–644.
6. Hutson, M. S., S. A. Hauger, and G. Edwards. 2002. Thermal diffusion and chemical kinetics in laminar biomaterial due to heating by a free-electron laser. *Phys. Rev. E Stat. Nonlin. Soft Matter Phys.* 65:061906.
7. Edwards, G. S., and M. S. Hutson. 2003. Advantage of the Mark-III FEL for biophysical research and biomedical applications. *J. Synchrotron Radiat.* 10:354–357.
8. Hutson, M. S., and G. S. Edwards. 2003. Advances in the physical understanding of laser surgery at 6.45 microns. *In* 26th International Free Electron Laser Conference and 11th FEL Users Workshop, Trieste, Italy. FRAIS01.
9. Xiao, Y., M. Guo, K. Parker, and M. S. Hutson. 2006. Wavelength-dependent collagen fragmentation during mid-IR laser ablation. *Biophys. J.* 91:1424–1432.

10. Spörl, E., U. Genth, D. Schmalfuß, and T. Seiler. 1997. Thermomechanical behavior of the cornea. *Ger. J. Ophthalmol.* 5:322–327.

11. Auerhammer, J. M., R. Walker, A. F. G. van der Meer, and B. Jean. 1999. Dynamic behavior of photoablation products of corneal tissue in the mid-IR: a study with FELIX. *Appl. Phys. B.* 68:111–119.

12. Shanmugam, G., and P. L. Polavarapu. 2005. Film techniques for vibrational circular dichroism measurements. *Appl. Spectrosc.* 59:673–681.

13. Caswell, D. S., and T. G. Spiro. 1987. Proline signals in ultraviolet resonance Raman-spectra of proteins—*cis trans* isomerism in polyproline and ribonuclease-A. *J. Am. Chem. Soc.* 109:2796–2800.

14. Sarkar, S. K., P. E. Young, C. E. Sullivan, and D. A. Torchia. 1984. Detection of *cis* and *trans* X-Pro peptide-bonds in proteins by C-13 NMR—application to collagen. *Proc. Natl. Acad. Sci. USA.* 81:4800–4803.

15. Jenness, D. D., C. Sprecher, and W. C. Johnson. 1976. Circular-dichroism of collagen, gelatin, and poly(proline)II in vacuum ultraviolet. *Biopolymers.* 15:513–521.

16. Bass, L. S., N. Moazami, J. Pocsidio, M. C. Oz, P. Logerfo, and M. R. Treat. 1992. Changes in type-I collagen following laser-welding. *Lasers Surg. Med.* 12:500–505.

17. Madey, J. M. J. 1971. Stimulated emission of bremsstrahlung in a periodic magnetic field. *J. Appl. Phys.* 42:1906–1930.

18. Shanmugam, G., and P. L. Polavarapu. 2004. Vibrational circular dichroism of protein films. *J. Am. Chem. Soc.* 126:10292–10295.

19. Holmgren, S. K., L. E. Bretscher, K. M. Taylor, and R. T. Raines. 1999. A hyperstable collagen mimic. *Chem. Biol.* 6:63–70.

20. Tseng, S. C. G., D. Smuckler, and R. Stern. 1982. Comparison of collagen types in adult and fetal bovine corneas. *J. Biol. Chem.* 257: 2627–2633.

21. Komai, Y., and T. Ushiki. 1991. The 3-dimensional organization of collagen fibrils in the human cornea and sclera. *Invest. Ophthalmol. Vis. Sci.* 32:2244–2258.

22. Mizuno, A., M. Tsuji, K. Fujii, K. Kawauchi, and Y. Ozaki. 1994. Near-infrared Fourier-transform Raman-spectroscopic study of cornea and sclera. *Jpn. J. Ophthalmol.* 38:44–48.

23. Frushour, B. G., and J. L. Koenig. 1975. Raman-scattering of collagen, gelatin, and elastin. *Biopolymers.* 14:379–391.

24. Goheen, S. C., L. J. Lis, and J. W. Kauffman. 1978. Raman-spectroscopy of intact feline corneal collagen. *Biochim. Biophys. Acta.* 536:197–204.

25. Diem, M., R. S. Bhatnagar, M. E. Druyan, and V. Renugopalakrishnan. 1984. Solution-phase Raman-spectroscopic studies on synthetic collagen analogs—Prolyl-Prolyl-Glycine and (Prolyl-Prolyl-Glycine)$_{10}$. *Biopolymers.* 23:2955–2961.

26. Shim, M. G., and B. C. Wilson. 1996. The effects of ex vivo handling procedures on the near-infrared Raman spectra of normal mammalian tissues. *Photochem. Photobiol.* 63:662–671.

27. Susi, H., J. S. Ard, and R. J. Carroll. 1971. Infrared spectrum and water binding of collagen as a function of relative humidity. *Biopolymers.* 10: 1597–1604.

28. Kampmeier, J., B. Radt, R. Birngruber, and R. Brinkmann. 2000. Thermal and biomechanical parameters of porcine cornea. *Cornea.* 19: 355–363.

29. Schober, R., F. Ulrich, T. Sander, H. Durselen, and S. Hessel. 1986. Laser-induced alteration of collagen substructure allows microsurgical tissue welding. *Science.* 232:1421–1422.

30. Saitô, H., and M. Yokoi. 1992. A C-13 NMR-study on collagens in the solid-state—hydration dehydration-induced conformational change of collagen and detection of internal motions. *J. Biochem. (Tokyo).* 111: 376–382.

31. Harrington, W. F. 1958. Effect of neutral salts on the structure of collagen and gelatin. *Nature.* 181:997–998.

32. Noack, J., and A. Vogel. 1999. Laser-induced plasma formation in water at nanosecond to femtosecond time scales: Calculation of thresholds, absorption coefficients, and energy density. *IEEE J. Quantum Electron.* 35:1156–1167.

33. Vogel, A., J. Noack, K. Nahen, D. Theisen, S. Busch, U. Parlitz, D. X. Hammer, G. D. Noojin, B. A. Rockwell, and R. Birngruber. 1999. Energy balance of optical breakdown in water at nanosecond to femtosecond time scales. *Appl. Phys. B.* 68:271–280.

34. Mackanos, M. A., J. A. Kozub, D. L. Hachey, K. M. Joos, D. L. Ellis, and E. D. Jansen. 2005. The effect of free-electron laser pulse structure on mid-infrared soft-tissue ablation: biological effects. *Phys. Med. Biol.* 50:1885–1899.

35. Mayo, K. H., D. Parradiaz, J. B. McCarthy, and M. Chelberg. 1991. Cell-adhesion promoting peptide GVKGDKGNPGWPGAP from the collagen type-IV triple helix—*cis*/*trans* proline-induced multiple ^{1}H NMR conformations and evidence for a kg/pg multiple turn repeat motif in the all-*trans* proline state. *Biochemistry.* 30:8251–8267.

36. Sanderson, R. T. 1971. Chemical bonds and bond energy. Academic Press, New York.